INTERNATIONAL JOURNAL FOR NUMERICAL METHODS IN FLUIDS, VOL. 4, 421–439 (1984)

# FINITE ELEMENT SOLUTIONS FOR LAMINAR AND TURBULENT COMPRESSIBLE FLOW

K. SRINIVAS AND C. A. J. FLETCHER

*Department of Mechanical Engineering, University of Sydney, N.S.W.2006, Australia*

SUMMARY

The time-split finite element method is extended to compute laminar and turbulent flows with and without separation. The examples considered are the flows past trailing edges of a flat plate and a backward-facing step. Eddy viscosity models are used to represent effects of turbulence. It is found that the time-split method produces results in agreement with previous experimental and computational results. The eddy viscosity models employed are found to give accurate predictions in all regions of flow except downstream of reattachment.

KEY WORDS Laminar Flow Turbulent Flow Compressible Flow Separation Time-split Method Finite Element Method

## 1. INTRODUCTION

A time-split finite element method was introduced and applied to compute laminar separated flows.[1] This method, which can also be interpreted as an alternating direction implicit finite element method, is well suited to compute steady flows by an unsteady approach. Although both laminar and turbulent flows are considered in the present work, more emphasis is given to the computation of turbulent flows. The results reported here are part of a computational investigation of complex trailing-edge flows such as the flow behind an aerofoil.

In the present work, we have two objectives. First, to introduce the simplest model for the Reynolds stresses that can accurately predict gross features of a turbulent flow. For the flow over an aerofoil a typical gross feature of interest would be the modification of the body pressure distribution by the separated region. For the problems considered here we will be interested in such gross features as the mean velocity profiles and the length of the separated region but will not attempt to determine details of the turbulence structure. Thus an algebraic eddy viscosity model has been employed to represent effects of turbulence; its suitability to compute the flows of interest is discussed in the text. Second, we are interested in modelling the trailing edge flow problems but with geometric characterizations that allow a simple prescription of boundary conditions. To achieve these objectives we compute two flows—the flow past the trailing edge of a flat plate, typical of an unseparated flow, and the flow past a backward-facing step, typical of a separated flow. These examples, which can be considered standard, have received considerable attention in the past. These include the experiments of Chevray and Kovasznay,[2] Andreopoulos and Bradshaw[3] and computations of Viswanath *et al.*[4] for the flow past a flat plate. The work of Bradshaw and Wong,[5] Chandrasuda and Bradshaw,[6] Sinha *et al.*[7] are some of the recent experimental investigations of the flow past a backward-facing step.

The structure of the rest of this paper is as follows. The governing equations, the time-split

0271–2091/84/050421–19$01.90

*Received 1 November 1982*
*Revised 11 February 1983*

finite element method and the eddy viscosity model are described in Section 2. The specific problems considered, the appropriate boundary conditions and other computational details, such as mesh geometry and law of the wall, are explained in Section 3. The various velocity profiles, pressure distributions and shear stress profiles are presented and discussed in Section 4.

## 2. GOVERNING EQUATIONS, COMPUTATIONAL ALGORITHM AND EDDY VISCOSITY MODEL

### 2.1. *Governing equations*

The flows under consideration are assumed to be governed by the two-dimensional, compressible Navier–Stokes equations

$$\frac{\partial \bar{q}}{\partial t}+\frac{\partial \bar{F}}{\partial x}+\frac{\partial \bar{G}}{\partial y}=\frac{\partial^2 \bar{R}}{\partial x^2}+\frac{\partial^2 \bar{S}}{\partial x\,\partial y}+\frac{\partial^2 \bar{T}}{\partial y^2} \tag{1}$$

where

$$\begin{aligned}
\bar{q} &= \{\rho, \rho u, \rho v\} \\
\bar{F} &= \{\rho u, p+\rho u^2-\sigma_x, \rho uv-\tau_{xy}\} \\
\bar{G} &= \{\rho v, \rho uv-\tau_{xy}, p+\rho v^2-\sigma_y\} \\
\bar{R} &= \{\theta_\rho^d \rho, \tfrac{4}{3}\mu u, \mu v\} \\
\bar{S} &= \left\{0, \frac{\mu}{3} v, \frac{\mu}{3} u\right\} \\
\bar{T} &= \{\theta_\rho^d \rho, \mu u, \tfrac{4}{3}\mu v\}
\end{aligned} \tag{2}$$

$$\begin{aligned}
\sigma_x &= \tfrac{4}{3}\varepsilon u_x - \tfrac{2}{3}\varepsilon v_y \\
\sigma_y &= \tfrac{4}{3}\varepsilon v_y - \tfrac{2}{3}\varepsilon u_x \\
\tau_{xy} &= \varepsilon(u_y + v_x)
\end{aligned} \tag{3}$$

$\rho$ = density, $u$, $v$ = velocity components in $x$ and y directions, $p$ = pressure, $\sigma_x$, $\sigma_y$, $\tau_{xy}$ = Reynolds stresses, $\mu$ = molecular viscosity, $\varepsilon$ = eddy viscosity (see Section 2.3 for details).

The dissipative terms in the continuity equation $\theta_\rho^d \rho$ (non-dimensional $\theta = 10/Re$), are included to stabilize the numerical procedure. The present method is being developed for transonic flows where we do not expect the temperature gradients to be large. Hence molecular viscosity, $\mu$ is assumed to be constant.

It is further assumed that the temperature can be related to the velocity by

$$T = T_0 - \frac{u^2+v^2}{2C_p} \tag{4}$$

so that the energy equation need not be solved. In equation (4), $C_p$ = specific heat at constant pressure, $T_0$ = stagnation temperature.

When equation (4) is combined with the ideal gas law, we get for the pressure,

$$p = \rho\left\{R_g T_0 - \frac{\gamma-1}{2\gamma}(u^2+v^2)\right\} \tag{5}$$

where $R_g$ = universal gas constant, $\gamma$ = ratio of specific heats.

Equation (5), which is exact for inviscid flows, is applicable to viscous flows when the Prandtl number is unity and there is no heat transfer at the body surface.

Equations (1)–(5) are non-dimensionalized with free stream values of density $\rho_\infty$, velocity $U_\infty$, and a characteristic length $L$. The governing equations retain the same form but for the following changes. $1/Re$ replaces $\mu$ where $Re = \rho_\infty U_\infty L/\mu$.

The pressure equation, when non-dimensionalized, becomes

$$1+\gamma M_\infty^2 p = \rho\{1+0{\cdot}5(\gamma-1)M_\infty(1-u^2-v^2)\} \tag{6}$$

where $M_\infty$ is the free stream Mach number.

### 2.2. *Time-split finite element method*

The time-split finite element method has been described in detail in Reference 1; here we give only the outline of the method. When we apply a Galerkin finite element formulation with linear, rectangular elements to the non-dimensional form of (1) we obtain the following system of ordinary differential equations,

$$\dot{\bar{q}} = \sum_{k,l} [f_{k,l}\bar{F}_{k,l} + g_{k,l}\bar{G}_{k,l} - r_{k,l}\bar{R}_{k,l} - s_{k,l}\bar{S}_{k,l} - t_{k,l}\bar{T}_{k,l}] = 0 \tag{7}$$

$k = i-1, i, i+1$ and $l = j-1, j, j+1$ (see Figure 1). $\bar{q}$ has components $\{\dot{\rho}_{i,j}, (\dot{\rho u})_{i,j}, (\dot{\rho v})_{i,j}\}$ after mass lumping. In equation (7) terms like $\bar{F}_{k,l}$ are the nodal values of $\bar{F}$. The coefficients $f$, $g$, $r$ depend only on the element geometry.

It may be noted that in forming equation (7), trial solutions have been assumed for groups of terms like $\rho uv$ that arise from the non-dimensional version of equation (1). It is shown by Fletcher[8] that the group finite element formulation[9] leads to significant gains in economy, without sacrificing accuracy. For the two-dimensional Burgers' equation solved by a time-split method with linear elements a reduction in execution times by a factor of 2 is achieved by the group formulation in comparison with the conventional finite element treatment of the convective terms.

Whereas the convective terms for Burgers' equation are quadratically non-linear, for compressible flow the non-linearity is cubic. For two-dimensional, compressible flow it is estimated[9] that the group formulation is approximately ten to fifteen times more economical than the conventional finite element method.

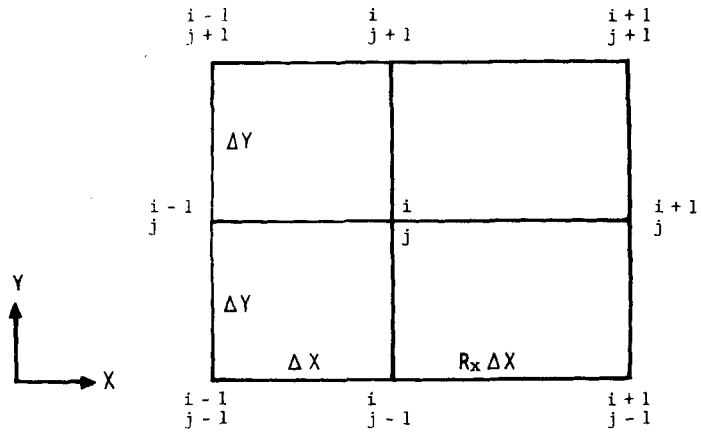


Figure 1. Nodal geometry

An ADI scheme is employed to solve the equations (7)

$$\bar{q}^* - \bar{q}^n + 0{\cdot}5\,\Delta t[\bar{F}_1^* + \bar{G}_1^n - \bar{R}_1^* - \bar{S}_1^n - \bar{T}_1^n] = 0 \tag{8}$$

$$\bar{q}^{n+1} - \bar{q}^* + 0{\cdot}5\,\Delta t[\bar{F}_1^* + \bar{G}_1^{n+1} - \bar{R}_1^* - \bar{S}_1^* - \bar{T}_1^{n+1}] = 0 \tag{9}$$

where $\bar{F}_1^*$ represents $\sum_{k,l} f_{k,l}\bar{F}_1^*$, etc.

It is necessary to introduce a linearization about the current time level if the tridiagonal algorithm is to be used to solve the above equations. This is carried out following Briley and McDonald.[10] Terms such as $(\rho u^2)^{n+1}$ are replaced by

$$\rho^{n+1}(u^2)^n + u^{n+1}2(\rho u)^n - 2(\rho u^2)^n \tag{10}$$

The solution has been sought as correction to the current solution $\rho^n$, $u^n$, $v^n$. The expressions such as (10) are replaced by

$$\Delta\rho^{n+1}(u^2)^n + \Delta u^{n+1}2(\rho u)^n + (\rho u^2)^n \tag{11}$$

equations (8) and (9) are thus written as

$$(\bar{H}^n + \bar{A}_x^n)\Delta\bar{p}^* = -0.5\,\Delta t\bar{R}_s^n \tag{12}$$

$$(\bar{H}^* + \bar{A}_y^*)\Delta\bar{p}^{n+1} = -0{\cdot}5\,\Delta t\bar{R}_s^* \tag{13}$$

where $\Delta p = \{\Delta\rho, \Delta u, \Delta v\}$. $H$ contains the contributions from the finite difference representation of $\dot{q}$. $A_x$ and $A_y$ are the contributions from the spatial terms such as $2(\rho u)$ that multiply the implicit terms in (11). $R_s$ is the residual of all spatial terms and approaches zero as the steady state is approached. This provides a convenient measure of the 'closeness' of the solution to the converged solution.

It can be shown that the method described is fourth-order accurate in space on a uniform grid for the inviscid terms.[1] It does not introduce any error other than that inherent in the finite element method. Further, the time-split method has the advantage that it allows the use of the efficient tridiagonal algorithm and that the demand on memory is modest. The stability properties of the method have been discussed in Reference 1.

### 2.3. *Eddy viscosity model*

The suitability of eddy viscosity models to compute turbulent flows has often been questioned. Although it is clear that the models cannot compute details of the turbulence structure, the previous applications do indicate that the models can, in fact, compute gross features of a flow quite satisfactorily.[11,12] Our interest is mainly in such gross features as the mean velocity profiles and skin friction distribution; eddy viscosity models are expected to be adequate for this purpose. However, doubts are often expressed as to whether eddy viscosity models can predict satisfactorily even the gross features of separated flow. One of the problems considered, i.e. flow past a backward-facing step involves a separated flow region as well as a reattaching region. Therefore it serves as a good example to test the eddy viscosity models for complex turbulent flows. The eddy viscosity model employed is as follows.

*Boundary layers.* Inner region

$$\varepsilon_i = \rho k_1^2 y^2 D^2 |u_y| \tag{14}$$

where $k_1$ is the von Karman constant (0·41) and $D$ is the van Driest damping factor:

$$D = 1 - \exp[-y(\tau_w/\rho_w)^{1/2}/26\nu_w] \tag{15}$$

Outer region

$$\varepsilon_o = k_2 \rho U_{max} \delta^* \gamma \tag{16}$$

where $k = 0{\cdot}0168$, $\gamma = [1 + 5{\cdot}5(y/\delta)^6]^{-1}$ (intermittency), $\delta^* = \int_{y_{ds}}^{\delta} (1 - \rho u/(\rho U)_{max})\, dy$, $y_{ds} = y$ coordinate of the dividing streamline (for a boundary layer, $y_{ds} = y_{wall}$).

*Wakes.* The same formulation as for the outer region of the boundary layer is used. Further, a simple relaxation procuedure is employed to approximate the influence of upstream history and is described later.

*Separated region.* The model used in the separated region follows the one suggested by Deiwert.[13] The value of the eddy viscosity in the separated region is interpolated between the wall and the dividing streamline and is damped using the Van Driest damping factor.

$$\varepsilon_i = k_2 U_{max} \delta^* \{(y/y_{ds}) D\} \tag{17}$$

$$D = 1 - \exp\{-y(\tau_w/\rho_w)^{1/2}/26\nu_w\} \tag{18}$$

$y_{ds}$ = dividing streamline, $D$ = Van Driest damping factor.

It was found during computations that the eddy viscosity distribution was discontinuous at the boundaries when the above formulations were employed for the flow past a backward-facing step. This was particularly so at the rearward end of the separation bubble. However the relaxation carried out on the eddy viscosity distribution to take into account the upstream history effects of turbulence ensured a smoother distribution at the boundaries.

*Relaxation.* It is well known that in regions downstream of a flat plate and downstream of a step, turbulence is not in local equilibrium. With eddy viscosity models it is usual to take into account the upstream history of turbulence by carrying out a relaxation. In the present investigations the relaxation was carried out by the following formula

$$\varepsilon_{i,j} = \alpha \varepsilon'_{k,l} + (1 - \alpha) \bar{\varepsilon}_{i,j} \tag{19}$$

In (19) $\bar{\varepsilon}_{i,j}$ is the eddy viscosity value given by the equations (14) to (18) and $\varepsilon'_{k,l}$ is the value at an upstream location. The upstream location, $k$, $l$ was located by tracing back along the velocity vector at the point $(i, j)$. The value of eddy viscosity at this upstream location was obtained by a linear interpolation among the four corners of the element in which the upstream point was situated. This is consistent with the use of linear shape functions to derive equations (7). The relaxation parameter $\alpha$ was chosen to be 0·3 as is the usual practice.[12]

## 3. PROBLEMS CONSIDERED, BOUNDARY CONDITIONS AND COMPUTATIONAL DETAILS

### *3.1. Flow past the trailing edge of a flat plate*

We consider a flat plate which separates two streams. Downstream of the trailing edge the boundary layers from the two sides of the plate merge and a wake flow results. Depending upon the flow on either side of the plate the wake may be symmetric or asymmetric about its centre line. Both symmetric and asymmetric wakes are considered in the present study. Asymmetry may be a result of the free-stream velocities being different on the two sides of the plate or it may be due to the wall roughness being different on the two sides of the plate (Figure 2). We call these 'velocity asymmetry' and 'roughness asymmetry' respectively. The various cases of laminar and turbulent wakes considered are given in Table I.

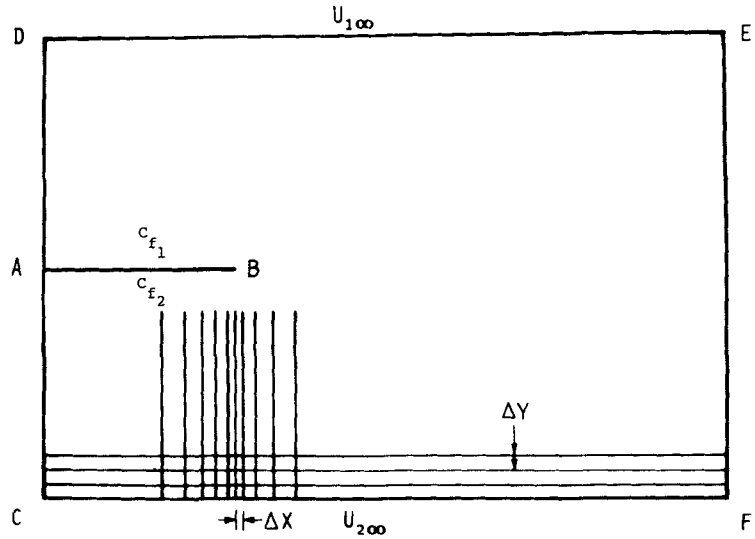


Figure 2. Boundary conditions and computational details for flow past trailing-edge of a flat plate (not to scale)

3.1.1. *Boundary conditions.* The boundary conditions applied are as follows (Figure 2):
On AB

$$u = v = 0 \tag{20}$$

On CD, the velocity components $u$ and $v$ are specified. Pressure is calculated from the extrapolation of the outgoing characteristic variable[14]

$$p_1^{n+1} = p_2^{n+1} - \rho_1^n c_1^n (u_2^{n+1} - u_1^{n+1}) \tag{21}$$

where $c$ is the speed of sound.

On DE, FC values of $\rho$, $u$ are prescribed at their non-dimensional free stream values, i.e. 1·0.

On EF, being an outflow boundary, the following conditions on $u$ and $v$ are applied

$$\frac{\partial^2 u}{\partial x^2} = \frac{\partial^2 v}{\partial x^2} = 0 \tag{22}$$

Table I. Examples considered for the flow past the trailing edge of a flat plate; Mach number in each case was 0·4. Refer to Figure 2 for a description of symbols

| | Laminar | | | Turbulent | | |
|---|---|---|---|---|---|---|
| Example | $Re_L$ | $U_{1\infty}/U_{2\infty}$ | $C_{f_1}/C_{f_2}$ | $Re_L$ | $U_{1\infty}/U_{2\infty}$ | $C_{f_1}/C_{f_2}$ |
| Symmetric wake | 100 | 1·0 | 1·0 | $10^6$ | 1·0 | 1·0 |
| Asymmetric wake (velocity) | 100 | 0·8 | 1·0 | $10^6$ | 0·8 | 1·0 |
| Asymmetric wake (roughness) | | | | $10^6$ | 1·0 | 2·0 |

and pressure is calculated from the non-reflecting condition

$$p_N^{n+1} = [p_N^n + \alpha \Delta t p_\infty + \rho_N^n c_N^n (u_N^{n+1} - u_N^n)] \frac{1}{1+\beta \Delta t} \tag{23}$$

A detailed discussion of this non-reflecting boundary condition is available in Reference 14. One of the important properties of this condition is that it reduces reflections at the outflow boundary of spurious disturbances generated by the transient solution. Consequently a faster convergence is achieved. In the same study it is found that $\beta = 0{\cdot}3$ gives good results and is therefore used in the present work.

3.1.2. *Computational details.* The flow was computed using a $34 \times 42$ mesh in the region CDEF (Figure 2). The plate AB, which had no thickness was placed in the centre of the region and it occupied 7 elements in the $x$-direction. The boundary DE was placed 2 boundary layer thicknesses away from AB. A uniform mesh of thickness 10 per cent of the inflow boundary layer thickness was employed in the $y$-direction. In the $x$-direction the mesh was graded to ensure a good resolution of flow both in the near wake and in the far wake. The smallest grid was set at the trailing-edge where its thickness was 10 per cent of the inflow boundary layer thickness. The mesh was stretched geometrically in the positive $x$ direction so that $\Delta x_{i+1}/\Delta x_i = 1{\cdot}3$. This stretching was also carried out in the upstream direction from the trailing edge B.

### *3.2. Flow past a backward-facing step*

This has become one of the benchmark flows involving separation and has received much attention in the past.[5,6,15] The flow over the step separates downstream of the corner (B in Figure 3) and gives rise to a mixing layer between the separation bubble and the outer flow. Downstream of the bubble the flow reattaches. The length of the separation bubble, the extent of reattachment, the pressure distribution through reattachment are some of the features of importance. Here again both laminar and turbulent flows are considered (Figure 3).

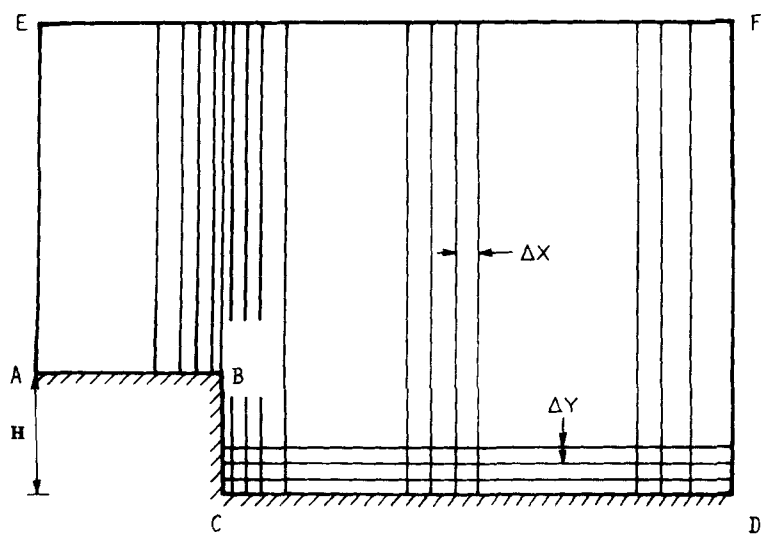


Figure 3. Boundary conditions and computational details for flow past a backward-facing step (not to scale)

3.2.1. *Boundary conditions.* The boundary conditions applied along AB, BC, CD, AE, EF (Figure 3) are similar to the ones applied along corresponding boundaries for the flat plate flow. The boundary conditions imposed along DF are that the first derivatives of $u$, $v$ and $\rho$ vanish at that boundary. This follows the conclusion of Fletcher[1] after experiments with a number of boundary conditions for the flow past a step. Such a condition is strictly not valid in boundary layer regions and was not imposed in the region adjacent to the wall, i.e. the two mesh points closest to the wall.

3.2.2. *Computational details.* The mesh employed is shown in Figure 3. $34 \times 42$ elements were used with the step occupying 10 in both $x$ and y directions. The boundary EF was placed three step heights away from AB. The mesh was uniform in the y direction, the mesh width being 10 per cent of the upstream boundary layer thickness. A variable mesh was used in the $x$ direction with the smallest mesh ($=\Delta y$) adjacent to the step. The mesh was stretched geometrically (mesh ratio = 1·3) up to about the rearward end of separation bubble. The region of the reattaching boundary layer had a uniform mesh (= upstream boundary layer thickness) followed by another region of geometrically stretched mesh (mesh ratio = 1·2). Such a mesh grading was necessary to ensure a good resolution of the flow features in the separating and the reattaching regions, without degrading the accuracy of the solution away from these regions, unnecessarily. The mesh was also stretched in the upstream direction from the corner B.

### *3.3. Law of the wall*

A good resolution of turbulent flows near walls requires a very fine mesh because of large velocity gradients. This would demand a large number of elements thus contributing to greater memory and time requirements on the computer. One way of overcoming this problem is to employ a law of the wall;[16] we have used this approach. Accordingly $u$ components of velocity at nodes adjacent to horizontal walls in the two examples considered are forced to satisfy the universal velocity profiles for turbulent boundary layers.

$$U^+ = Y^+, \qquad 0 < Y^+ < 5 \tag{24}$$

$$U^+ = (-3{\cdot}0 + 5{\cdot}0 \ln Y^+), \qquad 5 < Y^+ < 30 \tag{25}$$

$$U^+ = (-5{\cdot}0 + \ln Y^+/0{\cdot}41), \qquad Y^+ > 30 \tag{26}$$

where

$$Y^+ = \frac{yU_\tau}{\nu}, \qquad U^+ = U/U_\tau, \qquad U_\tau = \sqrt{(\tau_w/\rho)} \tag{27}$$

where $U_\tau$ = friction velocity, $\tau_w$ = wall shear stress, $\nu$ = kinematic viscosity.

This procedure was not carried out in regions downstream of the corner, B in the flow past the backward-facing step. In fact, it is not clear whether the velocity profiles follow any universal law in these regions.

## 4. RESULTS AND DISCUSSION

### *4.1. Flow past a flat plate*

Some of the preliminary results for this flow were presented previously.[17] Comparable results, to be discussed here, have been obtained with a refined mesh. In addition, many new cases are included.

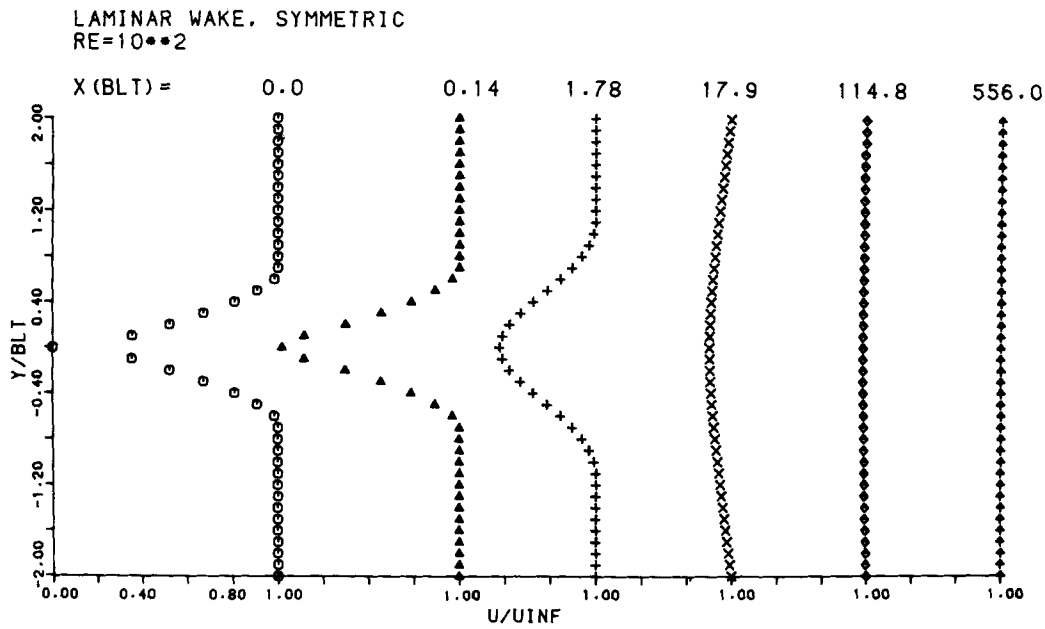


Figure 4. $U$-velocity profiles in laminar symmetric wake, $M_\infty = 0{\cdot}4$, BLT = boundary layer thickness at the trailing-edge

4.1.1. *Laminar flow.* Laminar flow past a flat plate was computed for a Reynolds number of 100 based on plate length. Computed $u$-velocity profiles at different locations downstream of the trailing-edge are given in Figure 4. The transformation of the boundary layer profile near the trailing-edge into a near wake profile and then its subsequent modification to a far-wake profile are well predicted. Self preservation of velocity profiles is one of the important properties of a wake, especially in the far-wake region. Figure 5 shows a plot of the velocity defect scaled to that at the centre-line varying with distance from the centre-line scaled to the half-wake width. Self preservation of the computational solution in the far wake region is clearly evident.

The velocity profiles for the velocity asymmetric laminar wake (Table I) are given in Figure 6. It is observed that the wake profile close to the plate slowly modifies itself into a mixing layer type profile as the downstream boundary is approached.

4.1.2. *Turbulent flow.* The turbulent flows were computed for a Reynolds number of $10^6$. Three flow cases, symmetric, velocity asymmetric and roughness asymmetric, were considered.

Symmetric wake:

The computed mean velocity profiles are shown in Figure 7. As expected, it is observed that most of the changes in the near-wake occur in the inner region and the outer region remains relatively unaffected. It is only towards the far wake that the outer region begins to change and assume a wake-like character. Investigations by Viswanath *et al.*,[4] though at a higher Reynolds number, i.e. $26{\cdot}6 \times 10^6$, provide a very good basis for comparison of the present results. Their investigations include experiments and computations with a $k$–$\omega^2$ model for turbulence. Some of the mean velocity profiles in the near-wake region are compared in Figure 8 with those of Viswanath *et al.*

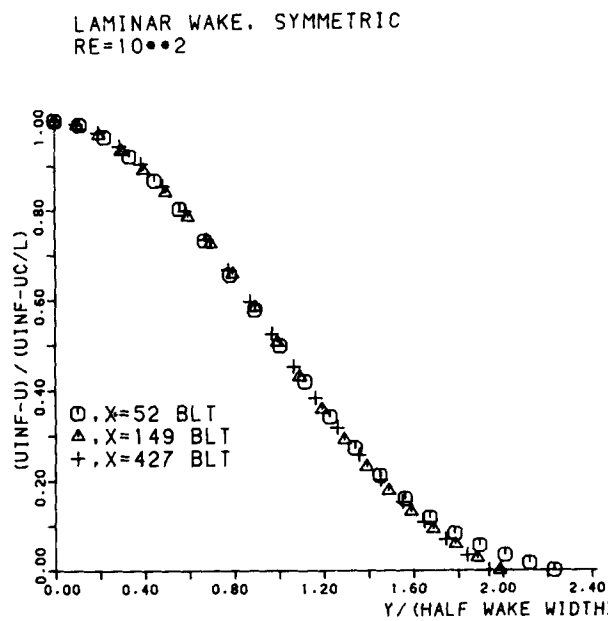


Figure 5. Self preservation of laminar symmetric wake, UC/L = $U$-velocity on the centreline of the wake

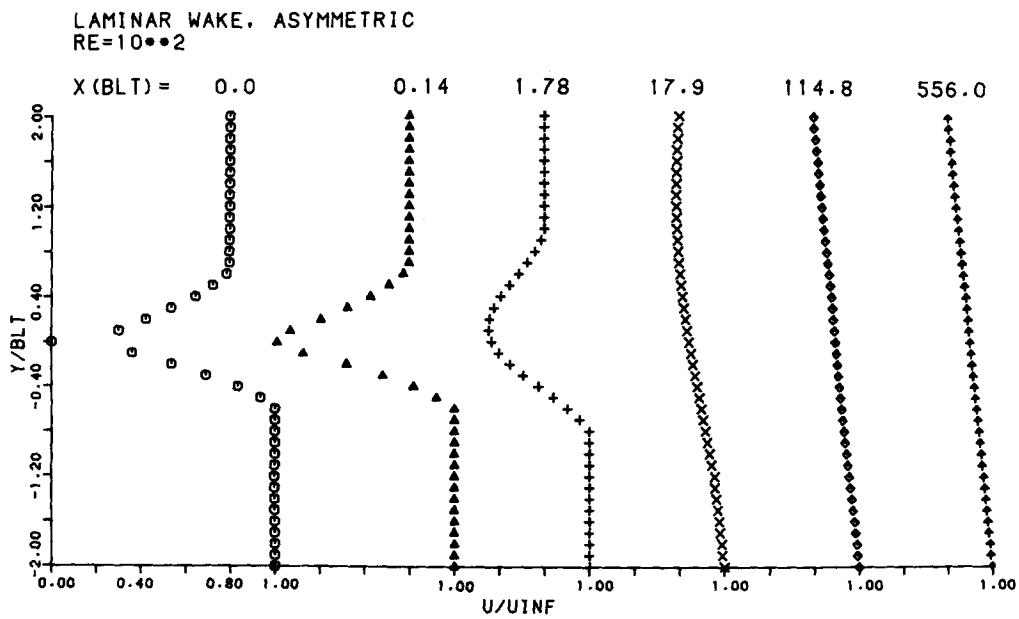


Figure 6. $U$-velocity profiles in laminar asymmetric wake, $M_\infty = 0{\cdot}4$, BLT = boundary layer thickness (lower) at the trailing-edge

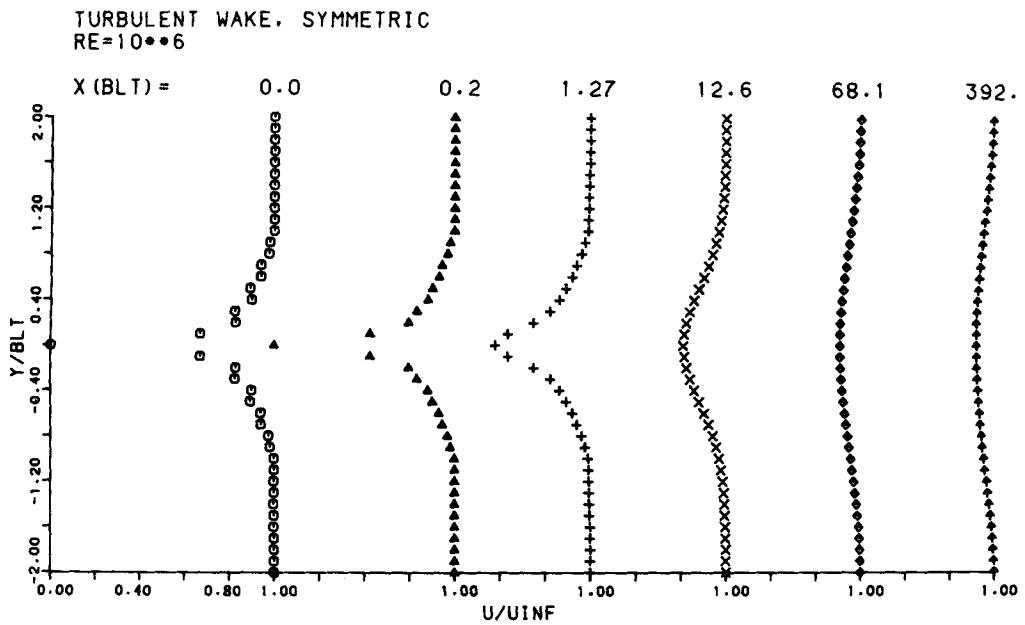


Figure 7. Mean $U$-velocity profiles in turbulent symmetric wake, $M_\infty = 0{\cdot}4$, BLT = boundary layer thickness at the trailing-edge

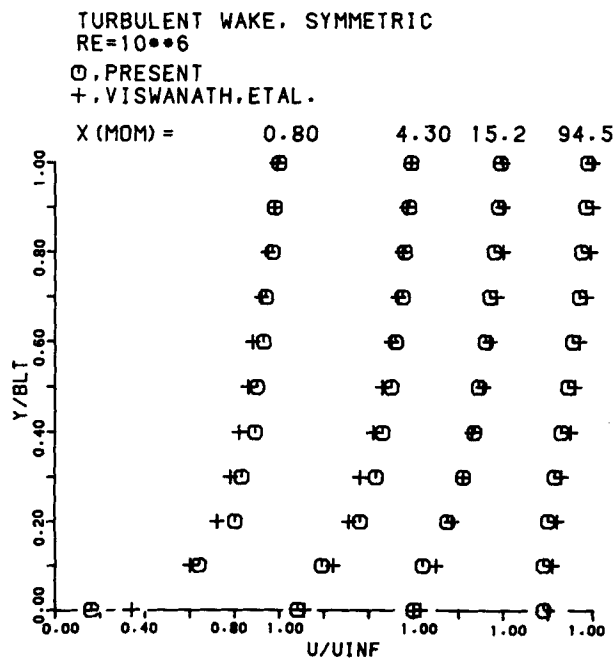


Figure 8. Comparison of velocity profiles in turbulent symmetric wake with those of Viswanath, *et al.*[4], ×(MOM) denotes distance from the trailing-edge measured in terms of momentum thickness at the trailing-edge

The present results agree very well with their experimental and computed results (computed results of Viswanath *et al.* are in very good agreement with those of their experiments) except for the profile at $x/\theta_0 = 0{\cdot}8$, (where $\theta_0$ = momentum thickness at the trailing edge). The disagreement is small in the outer layer but is considerable on the centre line. The magnitudes of mean velocities are 0·19 and about 0·3 in the present result and their result, respectively. The disagreement between the results at this specific location is probably explained by the differences in the geometries considered. We consider a flat plate of zero thickness whereas Viswanath *et al.* consider a 6·25° wedge. The effect of the wedge or flat plate is bound to be pronounced near the trailing-edge and should tend to vanish away from the trailing-edge. Further, the Reynolds numbers are different in the two cases under comparison.

The mesh employed in the $y$-direction in the present studies could also contribute to this difference. The location $x/\theta_0 = 0{\cdot}8$ is close to the trailing-edge of the plate where a boundary layer like flow prevails, and in this region we have used a coarser mesh than that used by Viswanath *et al.* For a good resolution in this region a fine mesh may be required in the $y$-direction. In the boundary layer region, however, the law of the wall was used to overcome the necessity of using a fine mesh.

The investigations of Viswanath *et al.* cover only the near-wake region and to compare our results in the far-wake region, we consider the experimental results of Chevray and Kovasznay[2] which have been obtained at a Reynolds number of $1{\cdot}5 \times 10^4$ based on the boundary layer thickness (compared to $2{\cdot}33 \times 10^4$ in the present case). The magnitudes of mean velocities at $x/\theta_0 = 258$ and 414 are 0·86 and 0·89 as against 0·83 and 0·89 measured by Chevray and Kovasznay. Thus we find that the present results are in substantial agreement with those measured or computed by others.

Self preservation of the computed mean velocity profiles is checked in Figure 9. It is found

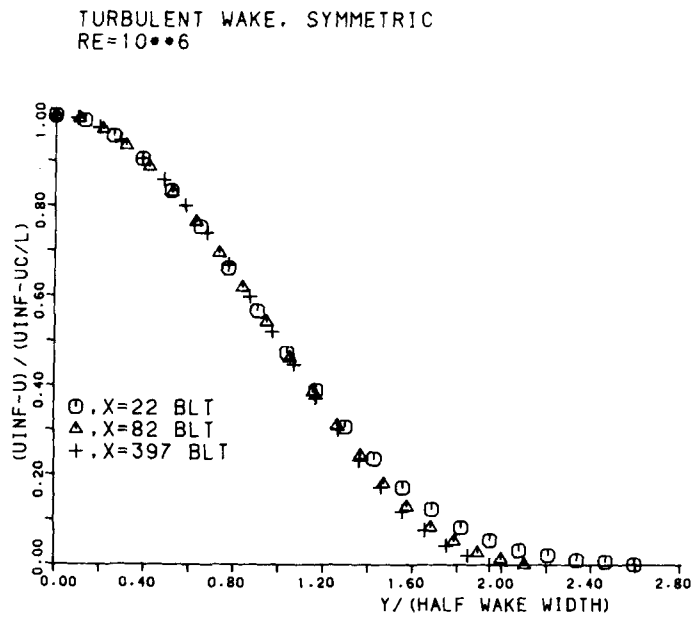


Figure 9. Self preservation of velocity profiles in turbulent symmetric wake, $M_\infty = 0{\cdot}4$, UC/L = $U$-velocity on the centreline of the wake

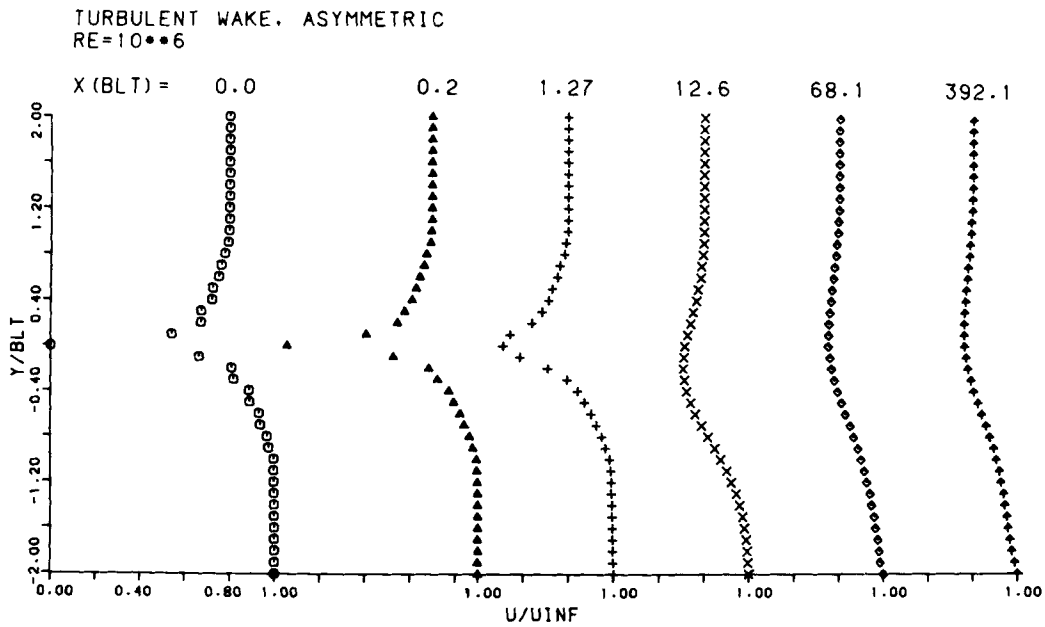


Figure 10. Mean $U$-velocity profiles in turbulent asymmetric (velocity) wake, $M_\infty = 0{\cdot}4$, BLT = boundary layer thickness (lower) at the trailing edge

that the profiles in the far wake do demonstrate self preservation except in the outer regions.

Velocity asymmetry:

The mean velocity profiles for the velocity asymmetric wake are given in Figure 10. As compared with the laminar asymmetric wake profiles, it is found that the modification of the far wake into a mixing layer is not complete. It is likely that proximity of the downstream boundary is contributing to this feature of the solution.

Roughness asymmmetry:

The roughness on the top surface of the plate was kept equal to twice that on the bottom surface of the plate. As a consequence of this the boundary layer thickness on the top surface increases by a factor of 1·4 and the universal velocity profile undergoes a shift by $-11U_\tau$.[3] The computed mean velocity profiles are given in Figure 11. It is found that the profiles which are asymmetric close to the trailing edge tend to become symmetric in the far-wake regions, as might be expected. A comparison of the eddy viscosity profiles in the wake regions with those obtained experimentally by Andreopoulos and Bradshaw[3] indicate a good qualitative agreement (profiles are not given in the present paper).

Thus we find that the eddy viscosity models can indeed compute wake flows satisfactorily. The results obtained are in good agreement with those obtained using the $k$–$\omega^2$ model of turbulence and with experimental results. The adequacy of the eddy viscosity models to compute such flows has also been noted in Reference 3. The agreement of the present results with those of Viswanath *et al.* also indicates that the accuracy of time-split finite element method compares well with that of the widely used MacCormack scheme (employed by Viswanath *et al.*). However, the present results have been obtained with less than half the number of mesh points used by Viswanath *et al.*[4]

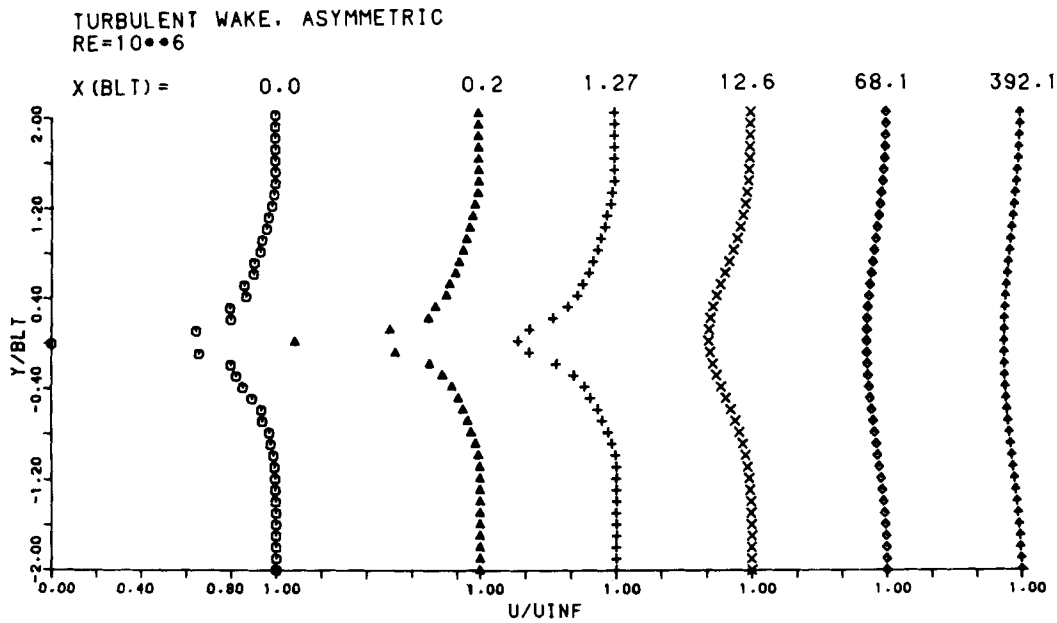


Figure 11. Mean $U$-velocity profiles in turbulent asymmetric (roughness) wake, $M_\infty = 0{\cdot}4$, BLT = boundary layer thickness (lower) at the trailing-edge

### 4.2. *Flow past a backward-facing step*

4.2.1. *Laminar flow.* The laminar flow past a backward-facing step was computed at a step-height Reynolds number of 53·0. The ratio of the boundary layer thickness at the step to the height of the step, i.e. $\delta/H$ was 1·0. The $u$ velocity profiles at various locations downstream of the step are plotted in Figure 12. The length of the separation bubble is 3·5 step-heights. This value is compared with those of previous investigators in Table II. The present value of 3·5 agrees closely with the least-square fit of Goldstein *et al.*[15] It may be pointed out that the least-square fit of Goldstein *et al.* takes into account the effect of the ratio of the step-height to the displacement thickness of the boundary layer.

Figure 12 shows that a sub-boundary layer starts building up downstream of the separation bubble. The extent to which this reattachment is complete is indicated by the shape factor. The shape factors of the boundary layer profiles at the step and at the downstream boundary were 2·62 and 2·42, respectively, thus indicating closeness to complete reattachment. Figure 13 gives the wall pressure distribution which we find to be in qualitative agreement with that given in Reference 7 for a step-height Reynolds number of 662.

4.2.1. *Turbulent flow.* The turbulent flow past the backward-facing step was computed for a step-height Reynolds number of $2{\cdot}3 \times 10^4$, the ratio $\delta/H$ being, again, equal to 1·0. This ratio corresponds to the 'strong perturbation' group according to the definition of Bradshaw and Wong.[5] 'Strong perturbation' implies that the turbulence structure is significantly altered during the flow.

We first discuss the wall pressure distribution and the maximum shear stress profile to be followed by a discussion of the mean velocity profiles.

Figure 13 gives the wall pressure distribution for the turbulent flow as well. The profile is in qualitative agreement with those given by Chandrasuda and Bradshaw[6] and Sinha *et al.*[7]

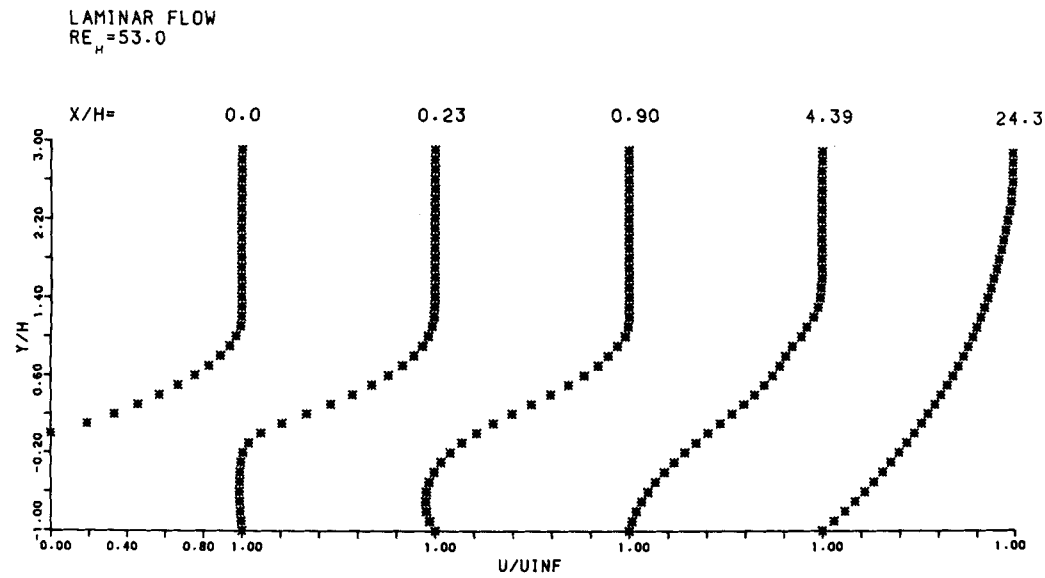


Figure 12. $U$-velocity profiles for laminar flow past the backward-facing step, $M_\infty = 0{\cdot}4$

The peak pressure coefficient at reattachment is 0·32 which is in reasonable agreement with Chandrasuda and Bradshaw[6] and with all of the computational results presented at the Stanford conference.[18]

The maximum shear stress values, given by $\varepsilon\left\{\frac{\partial u}{\partial y}+\frac{\partial v}{\partial x}\right\}$, are plotted in Figure 14. As noticed in experiments and other computations,[18] the shear stress starts to decay well ahead of the reattachment point (a discussion of the reattachment region follows). All of the computations in Reference 18 report that near reattachment the maximum shear stress reaches values much greater than in experiments. In the computations reported here the value of maximum shear stress near reattachment is $14{\cdot}0\times10^{-3}$ as against $11{\cdot}0\times10^{-3}$ observed during experiments.[18] The maximum shear stress value decays to about $8\times10^{-3}$ in about 5 step heights after reattachment whereas the corresponding value observed experimentally is $5\times10^{-3}$. The comparison of our computed shear stress values with those

Table II. Comparison of reattachment length for laminar flow, $Re = 53$

| Author | $X_r/H$ | Remarks |
|---|---|---|
| Leal and Acrivos* | 7 | |
| Goldstein, *et al.*[13] | 3·2 | from their least square fit |
| Mueller and O'Leary* | 4·5 | |
| Sinha, *et al.*[7] | 5·0 | extrapolated |
| Present | 3·5 | |

* The values of $X_r/H$ are taken from the graphs presented in Reference 7 and these references are not listed in the present paper. $X_r$ = reattachment length.

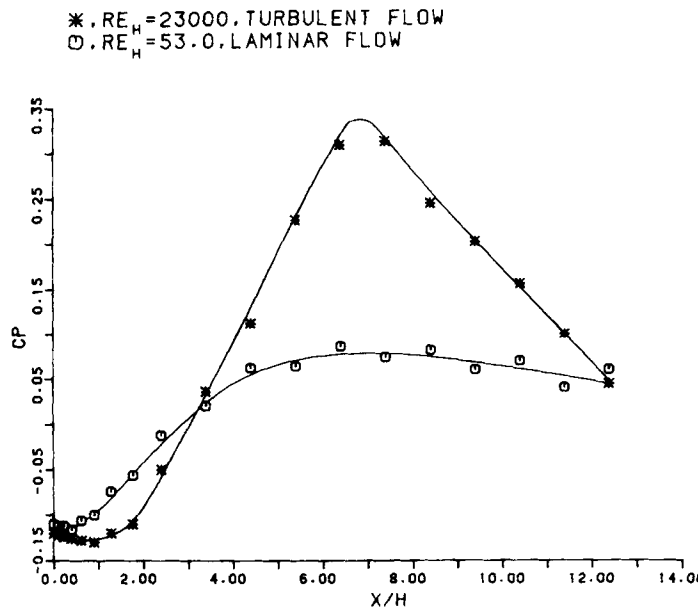


Figure 13. Wall pressure distribution

observed experimentally should be taken in a qualitative sense only because of the differences in Reynolds number and step-height to boundary layer thickness ratio of the computed and experimental cases.

Computed mean velocity profiles for various locations are given in Figure 15. Compared with the situation for laminar flow, reverse flow in the separated region is quite pronounced. The maximum reverse velocity is 0·253 of the free stream velocity and this value compares

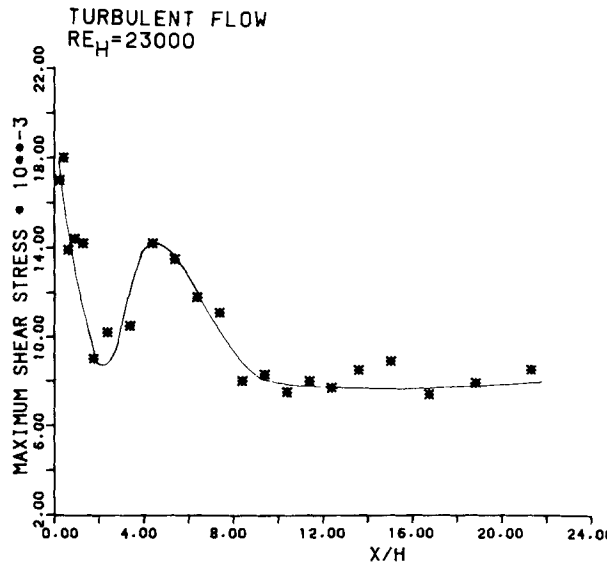


Figure 14. Distribution of maximum shear stress

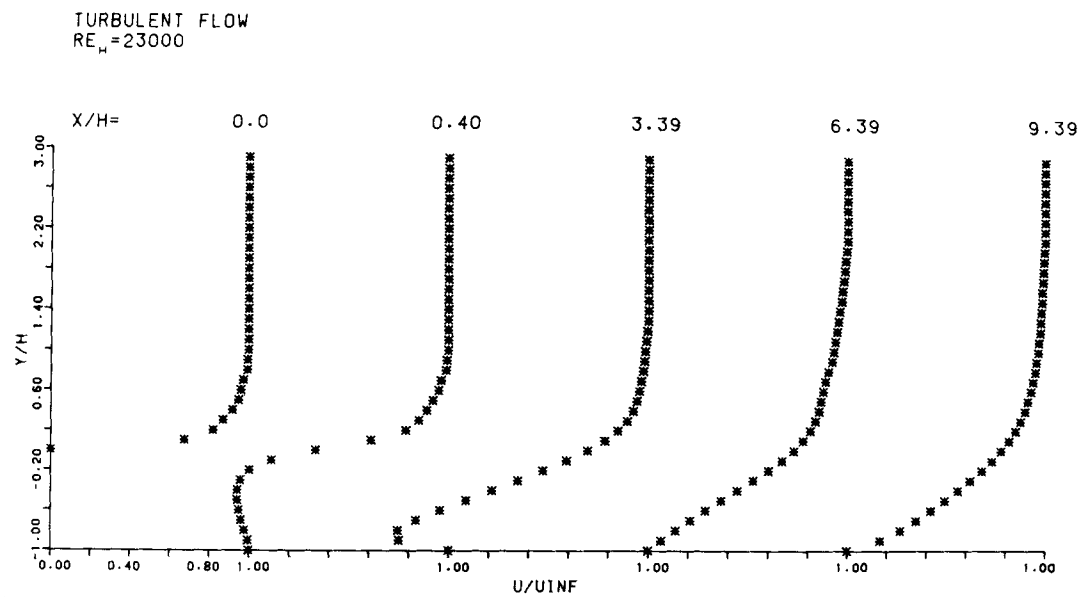


Figure 15. Mean $U$-velocity profiles for turbulent flow past the backward-facing step, $M_\infty = 0{\cdot}4$

well with the value of 0·28 given by Sinha *et al.*[7] The length of the separation bubble is found to be 5·5 step-heights. This is compared in Table III with the experimental values reported in the literature. Most of the modern measurements indicate a bubble length of 5 to 6 step-heights.

A recent study by Durst and Tropea[19] shows that the bubble length is strongly dependent on the expansion ratio (DF/AE in Figure 3) and Reynolds number, especially for channel flows (Table III). Their results indicate that for a step-height Reynolds number of $2{\cdot}3 \times 10^4$ (considered in the present study) and an expansion ratio of 1·14 (as against 1·0 in the present study) the bubble length is 5·2 step-heights. Other studies employing an expansion ratio of 1·0 have found the bubble length to be 4·5 and 5·2 step-heights (see Table III). Considering these, the bubble length obtained in the present studies, i.e. 5·5, seems quite reasonable.

Table III. Comparison of reattachment length for turbulent flow past the backward-facing step.

| Author | ER | $Re_H \times 10^4$ | $X_r/H$ |
|---|---|---|---|
| Tani, *et al.** | 1·01–11 | 0·3–11 | 7 |
| Mohsen* | 1·0 | 0·33 | 4·5 |
| Wauschkuhn and Vasata Ram* | 1·0 | 2·6–9·7 | 5·2 |
| Chandrasuda* | 1·65 | 10 | 5·85 |
| Eaton and Johnston* | 1·67 | 1·1–6·2 | 8·0 |
| Durst and Tropea[19] | 1·14–2·0 | 0·2–3·0 | 5·2–8·5 |
| Sinha, *et al.*[7] | 1·02–1·09 | 0·06–0·26 | 6·0 |
| Present | 1·0 | 2·3 | 5·5 |

* $X_r/H$ values are taken from the table presented in Reference 19 and the references are not listed in the present paper. ER = expansion ratio = DF/AE in Figure 3. $Re_H$ is step height Reynolds number.

Many of the computations reported in Reference 18 use differential equation models of turbulence and predict a bubble length of 5 to 6 step-heights for an expansion ratio of 1·5 and a step-height Reynolds number of $4\times10^4$. This is an underprediction of the experimental value of 7 for these conditions.

To determine the effect of reducing eddy viscosity in the separated region the following formula was used in place of (17)

$$\varepsilon_i = k_2 U_{\max}\, \delta^*[(y/y_{ds})D]^2 \tag{28}$$

It was found that the reduced eddy viscosity gave a slightly shorter bubble length (about 5 step-heights) and produced an unrealistic maximum reverse velocity of 0·410 at the rearward end of the bubble.

Reattachment of flow downstream of the separation bubble is another important feature of the flow considered. Results shown in Figure 15 correspond to a reattachment with a maximum skin friction coefficient of $10^{-3}$ as against $3\times10^{-3}$ upstream of the step. The corresponding shape factors were 1·37 and 1·92. The velocity profiles after reattachment are not predicted accurately. Such an observation has also been made by Horstman *et al.*[20] in their investigations of the flow past an aerofoil. The $k$–$\omega^2$ model, though better than the eddy viscosity models in this respect, is not very accurate either.[21]

Some improvement in predictions downstream of the separation bubble was achieved[21] by arbitrarily increasing the length scale of turbulence in the $k$–$\omega^2$ model. A similar attempt was made in the present studies by increasing the length scale arbitrarily in the outer layers after reattachment. The predictions of wall friction did improve considerably but the wall pressures calculated were not physically consistent with those of other parts of the flow field.

The reasons for the dubious behaviour of the eddy viscosity model after reattachment are not hard to find. The paper by Chandrasuda and Bradshaw[6] gives a clear description of the phenomenon of reattachment. The reattachment is characterized by the transport of turbulent energy and shear stress towards the surface, a large pressure strain term in the shear transport equation and dissipation and consequently a substantial decrease in shear stress and turbulent intensity downstream of reattachment. Clearly, such complex interactions are outside the scope of eddy viscosity models.

## 5. CONCLUSIONS

The time-split finite element method has been used to compute typical laminar and turbulent flows with and without separation. The examples considered were the flow past the trailing edge of a flat plate and the flow past a backward-facing step. Since the emphasis is mainly on gross features of the flow, eddy viscosity models have been used to model the effects of turbulence.

The method was found to compute the considered flows satisfactorily. One of the main questions under investigation was the suitability of eddy viscosity models to handle such flows. The results obtained for the flat plate flow are in very good agreement with those of others employing $k$–$\omega^2$ models of turbulence and with experimentally obtained results. For the flow past a backward-facing step results obtained using eddy viscosity models are accurate in all regions except downstream of reattachment. In this region the present computations underpredict skin friction but give an accurate prediction of the surface pressure distribution. The study therefore indicates that eddy viscosity models are effective except when details of the reattaching flow are important.

ACKNOWLEDGEMENTS

The authors are grateful to the Australian Research Grants Committee for their continued financial support. Thanks are also due to Mr. R. W. Fleet for his assistance in the preparation of drawings.

## REFERENCES

1. C. A. J. Fletcher, 'On an alternating direction implicit finite element method for flow problems', *Comp. Meth. Applied Mech. Engng.*, **30,** 307–322 (1982).
2. R. Chevray and L. S. G. Kovasznay, 'Turbulence measurements in the wake of a thin flat plate', *AIAA J.*, 1641–1643 (1969).
3. J. Andreopoulos and P. Bradshaw, 'Measurements of interacting turbulent shear layers in the near wake of a flat plate', *J. Fluid. Mech.*, **100,** Part 3, 639–668 (1980).
4. P. R. Viswanath, J. W. Cleary, H. L. Seegmiller and C. C. Horstman, 'Trailing-edge flows at high Reynolds number', *AIAA Paper 79-1503*, 1979.
5. P. Bradshaw and F. Y. F. Wong, 'The reattachment and relaxation of a turbulent shear layer', *J. Fluid Mech.*, **52,** 113–135 (1972).
6. C. Chandrasuda and P. Bradshaw, 'Turbulence structure of a reattaching mixing layer', *J. Fluid Mech.*, **110,** 171–194 (1981).
7. S. N. Sinha, A. K. Gupta and M. M. Oberai, 'Laminar separating flow over backsteps and cavities, part 1: backsteps', *AIAA J*, **19,** 1527–1530 (1981).
8. C. A. J. Fletcher, 'A comparison of finite element and finite difference solutions of the one and two-dimensional Burgers' equation', (to appear) *J. Comp. Phys.*, (1983).
9. C. A. J. Fletcher, 'The group finite element formulation', *Comp. Meth. in Appl. Mech. Eng.*, **37,** 225–243 (1983).
10. W. R. Briley and H. McDonald, 'Solution of the multidimensional compressible Navier–Stokes equations by a generalised implicit method', *J. Comp. Phys.*, **24,** 372–397 (1977).
11. J. D. Waskiewicz, J. S. Shang and W. L. Hankey, 'Numerical simulation of near wakes utilizing a relaxation turbulence model', *AIAA J*, **18,** 1440–1445 (1980).
12. G. S. Deiwert, 'Computation of turbulent near wake for asymmetric airfoils', *NASA Technical Memorandum 78581*, March 1979.
13. G. S. Deiwert, 'Computation of separated transonic turbulent flows', *AIAA J*, **14,** 735–740 (1976).
14. D. H. Rudy and J. C. Strikwerda, 'Boundary conditions for subsonic compressible Navier–Stokes calculations', *Computers and Fluids*, **9,** 327–338 (1981).
15. R. J. Goldstein, V. L. Eriksen, R. M. Olson and E. R. G. Eckert, 'Laminar separation, reattachment and transition of the flow over a downstream-facing step', *J. Basic Engng., Trans. A.S.M.E.*, 732–741 (1970).
16. C. E. Thomas, K. Morgan and C. Taylor, 'A finite element analysis of flow over a backward-facing step', *Computers and Fluids*, **9,** 265–278 (1981).
17. K. Srinivas and C. A. J. Fletcher, 'Application of alternating direction implicit finite element method to mixing flows', in P. J. Hoadley and L. K. Stevens (eds) *Finite Element Methods in Engineering, Proceedings of the Fourth International Conference in Australia on Finite Element Methods*, University of Melbourne, Australia, 18–20 August 1982, pp. 69–73.
18. J. K. Eaton, 'Summary of computations for case 0421-backward-facing step flow', *1980–81 AFOSR-HTTM-Stanford Conference on Complex Turbulent Flows.*
19. F. Durst and C. Tropea, 'Turbulent, backward-facing step flows in two-dimensional ducts and channels', *Third Symposium on Turbulent Shear Flows*, University of California, Davis, 1981.
20. C. C. Horstman, G. S. Settles, I. E. Vas, S. M. Bogdonoff and C. M. Hung, 'Reynolds number effects on shock wave boundary-layer interactions', *AIAA J*, **15,** 1152–1158 (1977).
21. C. C. Horstman, G. S. Settles, D. R. Williams and S. M. Bogdonoff, 'A reattaching free shear layer in compressible turbulent flow', *AIAA J.*, **20,** 79–85 (1982).